Journal of The Electrochemical Society, **157** (1) A98-A104 (2010)
0013-4651/2009/157(1)/A98/7/$28.00 © The Electrochemical Society

Continuum Representation for Simulating Discrete Events of Battery Operation

Vijayasekaran Boovaragavan,[a,*,] Venkatasailanathan Ramadesigan,[b,*] Mahesh V. Panchagnula,[c] and Venkat R. Subramanian[b,***,z]**

[a]*Department of Chemical Engineering and* [c]*Department of Mechanical Engineering, Tennessee Technological University, Cookeville, Tennessee 38505, USA*
[b]*Department of Energy, Environmental and Chemical Engineering, Washington University, Saint Louis, Missouri 63130, USA*

A mathematical approach for representing the discrete events in the cycling studies of lithium-ion batteries as a continuum event has been proposed to generate charge/discharge curves for *N* number of battery cycles. Simulations of up to 5000 cycles have been performed using this technique using the solid-phase diffusion model. A nonlinear electrochemical engineering model, which describes the galvanostatic charge/open-circuit/discharge processes of a thin-film nickel electrode, has also been investigated to test and validate the computational performance of the continuum representation technique. Finally, the tested technique is implemented for an existing full-order pseudo-two-dimensional lithium-ion battery model that has several coupled and nonlinear partial differential equations in multiple domains. The continuum representation, which is expressed as a function of a dependent variable in time *t*, works efficiently for several cycles with very minimal model initialization efforts and computation cost. However, it is not ideal for state detection.
 [DOI: 10.1149/1.3258044]

Manuscript submitted February 19, 2009; revised manuscript received September 21, 2009. Published November 24, 2009.

The mathematical simulation approaches that are currently followed for the modeling of charge/discharge cycles of lithium-ion batteries involve different computational schemes.[1-10] The complexity arises because of steep variations in the dependent variables (concentrations and potentials) between charge and discharge processes, difficulty in obtaining consistent initial values for the model equations, solver failure after a certain number of cycles due to high charge/discharge cutoff voltages, thermal effects, etc. We came up with a shooting method in a spatial direction[11] based on the steady-state model equations that work well for providing consistent initialization during a charge or discharge process. Wu and White[12] devised an initialization subroutine called differential algebraic equation initialization subroutine (DAEIS) to overcome numerical inconsistency and discussed in detail the initialization problems of battery models. Consistent initial values of the dependent variables for index-1 differential algebraic equation (DAE) systems can be obtained using DAEIS. DAEIS is effective in handling a DAE system with combined continuous processes and discrete events that are frequently encountered in battery operations. Before the advancement of computation capability, Tafel approximation of the electrokinetic expression and Ohm's law in electrolyte were used to calculate initial guesses for algebraic variables.[13]

In this work, the complete protocol that includes many discrete events to constitute one cycle of lithium-ion battery was reformulated as a single continuous process. Then, this continuous process was repeatedly simulated up to the desired number of cycles. This was achieved by carefully changing the model variables that directly influence the cycling parameters, for example, changing the independent variable (in time) or the dependent variable (in solid-phase concentration at the surface of the intercalating particles) and expressing the same as an additional algebraic equation in terms of the number of battery cycles. This approach was attempted to overcome the difficulties mentioned during the conventional cycle studies, and it was an efficient method for many situations. Adding an additional nonlinear algebraic equation does not contribute to the significant computation cost for the model simulation; rather, it helps in effectively handling large cycle numbers and in generating the cycle data for further analysis.

The proposed mathematical representation has been demonstrated for models with different degrees of complexity and in comparison with the results from those using the conventional approach.[1-4] First, a simple model that governs the solid-phase diffusion was demonstrated to explain the approach. Then, the nonlinear model that was used as an illustrative problem for the inconsistent initialization problem[12] was used to generate the cycle data with this approach. Finally, the full-order physics-based pseudo-two-dimensional model of the lithium-ion battery[1-10] was studied for up to 1000 cycles. For the purpose of cycling or parameter estimation using the full-order physics-based lithium-ion battery model, we devised an efficient reformulated model of the full-order model, and the details of this reformulation and the related mathematical techniques are partly discussed elsewhere.[14-16] The combination of this continuum representation and this efficient reformulated model helps in the use of meaningful models of batteries for emerging applications such as satellites, military, hybrid electric vehicles, etc. The combination of the continuum representation and the reformulated model is helpful in a way that solving the full-order physics-based lithium-ion battery model with less computation cost was facilitated by the reformulated version of the full-order model that does not require a large system of differential and algebraic equations to be solved for each parameter in a cycle, for example, charge or discharge. Though the objective of this investigation is to devise a continuum representation for generating cycle data using a full-order physics-based lithium-ion battery model, two other simple electrochemical models (mentioned above) are also discussed with the intention to provide more details and insight into the proposed continuum approach that can help readers to easily adopt the approach for other interesting cases.

Numerical Routines for Continuum Representation

Electrochemical engineering models for batteries are usually solved using the finite difference method that typically represents a system of DAEs with first-order differential equations in time and known or fixed initial conditions. The algebraic equations come from the finite difference form of the electronic and ionic conduction equations, charge balance, and boundary conditions with unknown initial values. As a consequence, a dedicated numerical routine with consistent initial values must be adopted when solving these stiff DAE systems. Recently, there are many numerical DAE solvers, such as DASSL,[17] DASPK,[18] BzzDae,[19] LIMEX,[20] Jacobian,[21] gPROMS,[22] DAESOL,[23] and SPRINT,[24] introduced in the literature. The real world simulations involve variables that are physically bound. The routines that are able to deal with constraints are DASPK, BzzDae, Jacobian, and gPROMS. Although, ready-

* Electrochemical Society Student Member.
** ECS Oronzio de Nora Industrial Electrochemistry Fellowship Award Recipient.
*** Electrochemical Society Active Member.
z E-mail: vsubramanian@seas.wustl.edu

made solvers are available with constraint handling options, the studies on the cycling performance of batteries needs tweaking of the solvers to achieve better efficiency and robustness. The continuum representation proposed is based on tweaking any DAE solver using a proper combination of hyperbolic functions. Additional literature dealing with embedded analytical solutions and discretization methods, which might help researchers dealing with such reformulation models, is given elsewhere.[25,26]

Solid-State Diffusion Model

To illustrate the working principle of continuum representation and charge/discharge modeling, we start with a simple diffusion model that governs the electrochemical behavior of the solid-phase active materials in porous electrodes. The species transport in a spherical electrode can be expressed in a dimensionless form as

$$\frac{\partial C}{\partial \tau} = \frac{1}{X^2}\frac{\partial}{\partial \tau}\left(X^2\frac{\partial C}{\partial X}\right) \quad [1]$$

with the boundary conditions

$$\frac{dC}{dX} = 0 \quad \text{at } X = 0 \text{ and for } \tau \geq 0 \quad [2]$$

$$\frac{dC}{dX} = \delta \quad \text{at } X = 1 \text{ and for } \tau \geq 0 \quad [3]$$

and initial condition

$$C = C_{\text{ref}} \quad \text{at } \tau = 0 \text{ and for } 0 \leq X \leq 1 \quad [4]$$

where δ is the applied current density in dimensionless form. Here, the electrochemical model is assumed to have a cycling protocol that consists of charging at constant current, followed by rest, and discharging at constant current. The charge/discharge cutoff potentials are evaluated using the Nernst equation based on the surface concentration. The equilibrium potential was assumed to be equal to 4.2 V (similar to the voltage expected in the lithium-based battery materials).

The three discrete processes above can be treated as one continuous event using a combination of hyperbolic functions

$$f = \frac{1 - \tanh[k(\tau - 0.2)]}{2} - \frac{1 - \tanh(k\tau)}{2} \quad [5]$$

A plot for this function (Eq. 5) against time, τ is shown in Fig. 1a for different values of the parameter k. Equation 5 maintains a fixed value for f that ranges between the time interval of 0 and 0.2. The parameter k is important if a dimensionless form of τ is used, and it varies between 0 and 1. However, for higher values of τ, like in the range of 100 s or above, k can take a value of 1. This is shown in Fig. 1b. If it is desired to analyze the cycling performance of two or three different parameters over one or N number of cycles, then it is straightforward to follow from Eq. 5 that adding some additional functions serves the purpose

$$F = \sum_{i=1}^{N} f(i) \quad [6]$$

Figure 1c shows the schematic of discrete processes that are combined together as a function of the independent variable time, t. For instance, a protocol with charging at a particular current for $\tau = 1000$, followed by leaving it at open circuit until the potential stabilizes (say, another 1000 units) and discharging at constant current for 1000 units, can be represented in continuum form as given below

$$\delta = (s_2 - s_1)\delta_c + (s_3 - s_2)\delta_{oc} - (s_4 - s_3)\delta_d \quad [7a]$$

$$s_1 = \frac{1 - \tanh(\tau)}{2} \quad [7b]$$

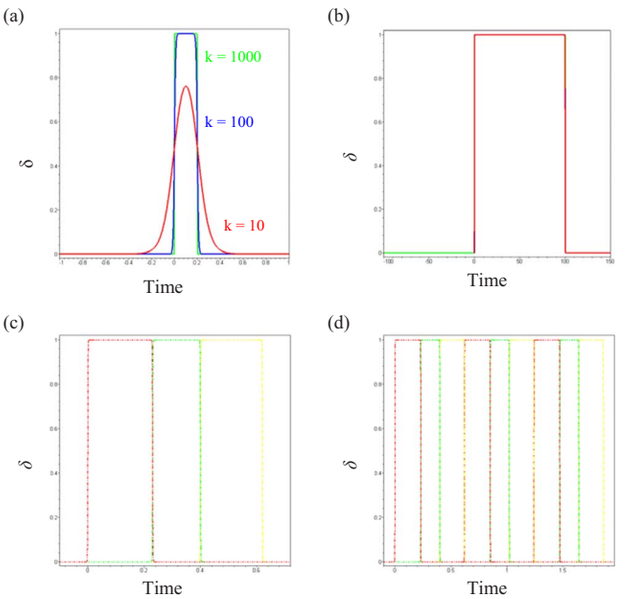

Figure 1. (Color online) Plot of the function (Eq. 1) (a) for various k values, (b) for higher values of time, t, (c) for one cycle consisting of three parameters, and (d) for N number of cycles.

$$s_2 = \frac{1 - \tanh(\tau - 1000)}{2} \quad [7c]$$

$$s_3 = \frac{1 - \tanh(\tau - 2000)}{2} \quad [7d]$$

$$s_4 = \frac{1 - \tanh(\tau - 3000)}{2} \quad [7e]$$

$$\delta_{oc} = \left.\frac{dC}{dX}\right|_{X=1} \quad [7f]$$

where δ_c is the dimensionless applied charging current, δ_{oc} is the dimensionless open-circuit current (the value of which can be calculated using Eq. 7f), and δ_d is the dimensionless applied discharge current. Figure 1d shows the behavior of Eq. 7 as a function of the cycling period. It is clear from these figures that when the solver solves for a cycling parameter (charging, discharging, or open circuit), it is automatically directed to the next parameter specified in the protocol. Sometimes a slight smoothness between the cycling parameters is introduced by adjusting the parameter k. This smoothness, as shown in Fig. 1a for $k = 10$, is important to overcome inconsistencies in stiff model initialization problems at the transition point in time. It is because the solver is given enough space in time (or state) domain to detect the next parameter in the cycling protocol at the transition point where the solver usually finds difficulty in convergence or often times fails. Thus, the parameter k also solves the inconsistencies in stiff model initialization problems at the transition point in time. Choosing such a value for k is one of the key factors for the error-free and nonstop generation of cycling data using the continuum representation approach. Usually, this short time span between any two cycling parameters is where the model undergoes steep variations in charge/open-circuit/discharge characteristics that add to computational difficulties.

The results from the simulation of one complete cycle using the continuum cycling approach (Eq. 5) are presented in Fig. 2. Figure 2a shows the applied current, and it is consistent with the defined cycling protocol. Figure 2b shows the corresponding terminal voltage–time curve, and Fig. 2c shows the surface concentration

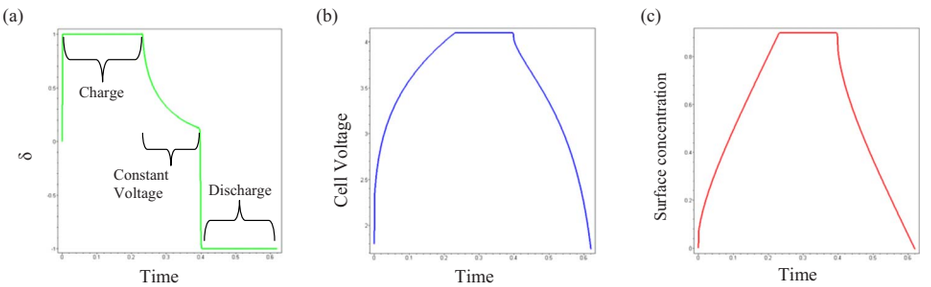

Figure 2. (Color online) (a) Current distribution, (b) potential distribution, and (c) concentration distributions from a cycle of a solid-phase diffusion model.

dynamics during the cycling process. These current, potential, and concentration curves are the results from cycle 1 of the solid-phase diffusion model. It shows that during constant current charge, the concentration of the active species inside the spherical particle increases across the spherical particle radius. Next, the surface concentration is maintained constant during constant voltage charge until the concentration achieves a uniform profile across the radial direction that can be evidenced from the transient current profile shown in Fig. 2b. This constant voltage step is handled by a fixed surface concentration and allowed the current to vary in accordance with the governing equations. The current as a function of time is then calculated in the postprocess steps, which is an unknown profile a priori during this cycle studies.

Equation 7 is used for the automated cycling of the model above for up to 1000 cycles. The cycling profiles between 500 and 510 cycles are shown in Fig. 3, and a comparison of the computational statistics for this simulation is given in Table I. Clearly, the use of an additional equation takes care of the sustained solver efficiency and provides data for N number of cycles. The computational cost could be twice or more than the values shown in Table I if one needs to stop the solver at each cycle or cycle parameter and to reinitiate the solver. All the simulations in this demonstration are performed in Visual Fortran and Maple environments using a PC with 2 GB RAM and a 2.4 GHz Pentium IV processor.

Thin-Film Nickel Hydroxide Electrode

The second example considered for the validation of the continuum representation technique is the cycle-life modeling of the galvanostatic charge, open-circuit, and discharge processes of a thin-film nickel hydroxide electrode as given[12]

$$\frac{\rho V}{W} y_1' = \frac{j_1}{F} \quad [8]$$

$$j_1 + j_2 - i_{\text{app}} = 0 \quad [9]$$

$$j_1 = i_{01}\left[2(1 - y_1)\exp\left(\frac{0.5F}{RT}(y_2 - \phi_{\text{eq},1})\right) - 2y_1 \exp\left(-\frac{0.5F}{RT}(y_2 - \phi_{\text{eq},1})\right)\right] \quad [10]$$

$$j_2 = i_{02}\left[\exp\left(\frac{F}{RT}(y_2 - \phi_{\text{eq},2})\right) - \exp\left(-\frac{F}{RT}(y_2 - \phi_{\text{eq},2})\right)\right] \quad [11]$$

The dependent variables y_1 and y_2 are the mole fraction of NiOOH and the potential difference at the solid/liquid interface, respectively. The values of the model parameters are $F = 96{,}487$, $R = 8.314$, $T = 298.15$, $\phi_{\text{eq},1} = 0.420$, $\phi_{\text{eq},2} = 0.303$, $\rho = 3.4$, $W = 92.7$, $V = 1 \times 10^{-5}$, $i_{01} = 1 \times 10^{-4}$, $i_{02} = 1 \times 10^{-10}$, and $i_{\text{app}} = 1 \times 10^{-5}$ (units of parameters omitted for simplicity). Previous work[12] reported that a consistent initialization is important for this DAE model even for a single run of the simulation. It was also observed that the popular DAE solvers such as DASSL and RADAU5 failed for one run of simulation with initialization error messages. By incorporating an additional algebraic equation as discussed in this charge/discharge modeling approach, the solver self-adjusted to nearly consistent initial values and continued to provide cycle data for up to 1000 cycles. Figure 4 shows the continuous simulation of the discrete events. The variations in both the concentration and potential as a function of time are shown for the first 46 cycles. The computational statistics associated with this simulation is also given in Table I. These results are consistent with the results of the simulation shown for 30 cycles in Fig. 2 elsewhere.[12]

Pseudo-Two-Dimensional Model of a Lithium-Ion Cell

The models for actual physical systems are usually more complex than the above two cases. Hence, a full-order pseudo-two-dimensional model for lithium-ion batteries, which is currently in practice,[1-10] was considered to test the validity of the proposed continuum representation approach. These models are the most promising candidates because they can predict both internal and external behaviors (system level) with reasonable accuracy. These models are based on the porous electrode theory coupled with transport phenomena and electrochemical reaction engineering. They are represented by coupled nonlinear partial differential equations (PDEs) in one to two dimensions and are typically solved numerically, requiring a few minutes to hours to simulate. A summary of the model equations for the behavior of lithium-ion batteries at various operating conditions for a wide range of chemistries is shown in Table II. The electrochemical modeling of a typical secondary battery involves three regions: the positive porous electrode, the separator, and the negative porous electrode. The original model involves 10 PDEs (4 in each electrode and 2 in the separator). If 100 node points are used in the x-direction in each region and 20 node points are used in the r-direction, the original model involves 2×100 (separator) $+ 3 \times 100$ (macroscale in each electrode) $+ 1 \times 20 \times 100$ (microscale in each electrode) $= 200 + 300 \times 2 + 2000 \times 2 = 4800$ DAEs in time. This model accounts for the diffusion and the reaction in the electrolyte phase in the anode/separator/cathode, the diffusion (intercalation) in the solid phase in the cathode and the anode, the ionic and electronic conductivities in the corresponding phases in the porous electrodes (cathode and anode), nonlinear ionic conductivity, the nonlinear kinetics, etc. The expressions and parameters used in the governing equations are given in Tables II-IV. This full-order model available in the literature[1-10] was validated with the experimental charge/discharge curves at various operating conditions. The protocol that is commonly used in cycling lithium-ion battery consists of charging the battery at a constant current up to a cutoff potential, followed by charging at a constant potential until the potential reaches a uniform value across the intercalating particles, and finally, discharging the battery at a constant current or potential. A better utilization of lithium-ion batteries can be obtained by discharging at low rates under galvanostatic conditions.

Figure 5 shows the charge/discharge behavior of the battery as a function of N at the 1C rate of charge or discharge for up to 100 cycles. The potentials for charge and discharge are allowed to vary between 4.2 and 3.05 V. This plot shows that the continuum representation works well for the practical battery model. In practice, the

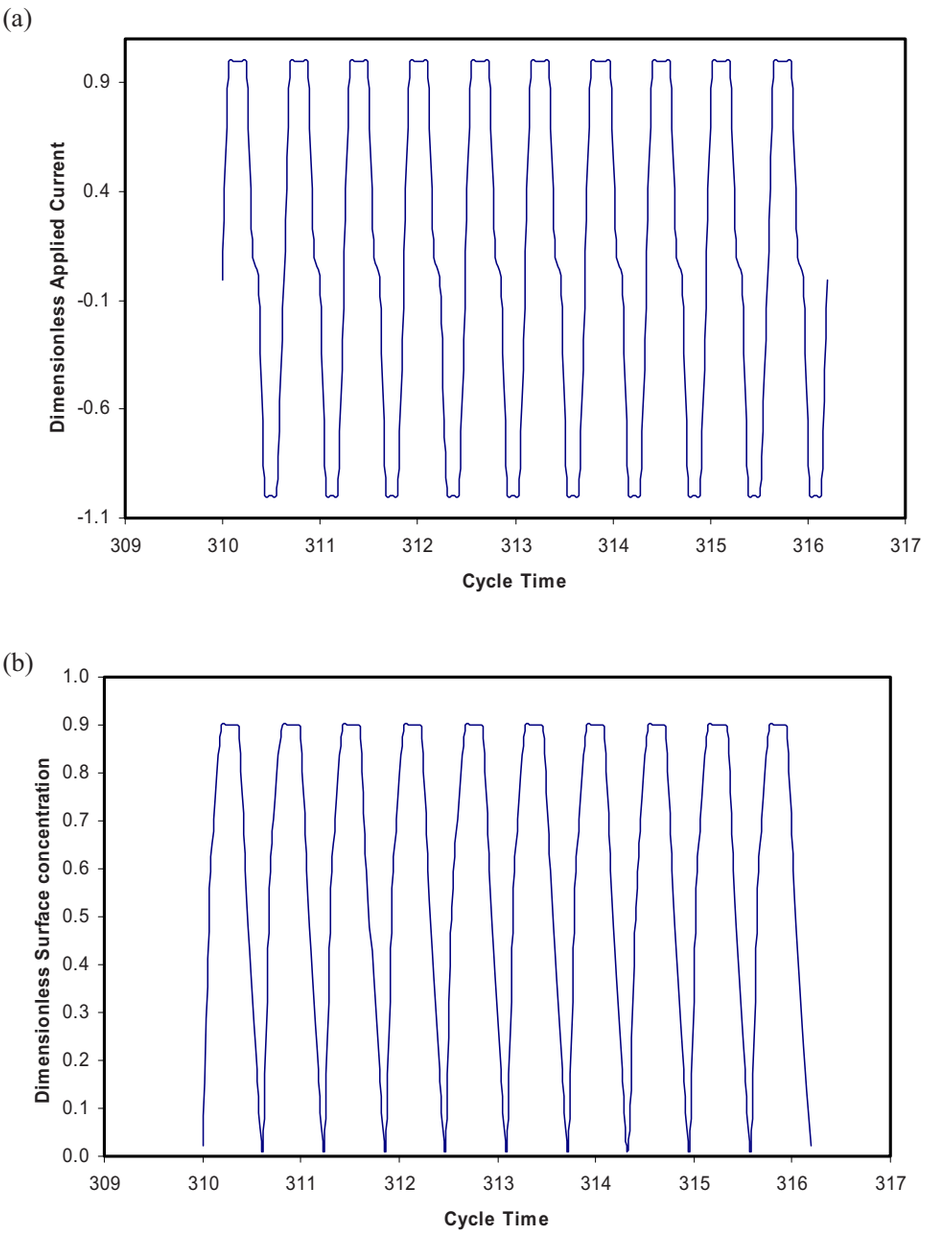

Figure 3. (Color online) (a) Current and (b) potential distributions between 500 and 510 cycles for a solid-phase diffusion model.

battery loses its capacity to hold and deliver the energy when the number of cycles increases.[27] This behavior can also be captured by incorporating a linear dependency for the diffusive conductivity of ionic species in the negative electrode. The capacity fade is mainly due to the variations in the transport and kinetic parameters caused by the reduced pore volume in the porous electrodes, which in turn increases the internal resistances for ionic/mass transport. The computational statistics for this full-order model are given in Table I. The simulation time is not proportional to the cycle number because if we run the battery model for one cycle, much of the CPU time is spent for the model initialization, and thus the final time taken for cycle 1 is larger compared to that for cycle 10, where the hyperbolic function accelerates the solver without getting struck or spending more time for the initialization. The proposed continuum representation technique works for a porous electrode model because the total current of the cell is constant, and the cell is operated under a galvanostatic condition. However, the nonuniform current density

Table I. Computational statistics for the modeling of cycling behavior using various models at 10, 100, and 1000 cycles.

Number of cycles	Solid-phase particle model (s)	Thin-film electrode model (s)	Full-order Li-ion model (s)
10	0.89	0.219	128.47
100	28.86	2.019	1286.25
1000	1988.22	191.281	15896.53

Table II. Governing equations for a lithium-ion cell based on the porous electrode theory.

Region	Equation number	Governing equations	Boundary conditions
Positive electrode	1	$\varepsilon_p \partial c/\partial t = D_{\text{eff,p}} \partial^2 c/\partial x^2 + a_p(1-t_+) j_p$ Initial condition $c\|_{t=0} = c_0$	$-D_{\text{eff,p}} \partial c/\partial x\|_{x=0} = 0$ and $-D_{\text{eff,p}} \partial c/\partial x\|_{x=l_{p^-}} = -D_{\text{eff,s}} \partial c/\partial x\|_{x=l_{p^-}}$
	2	$-\sigma_{\text{eff,p}} \partial\Phi_1/\partial x - \kappa_{\text{eff,p}} \partial\Phi_2/\partial x + 2\kappa_{\text{eff,p}} RT/F(1-t_+) \partial \ln c/\partial x = I$	$-\kappa_{\text{eff,p}} \partial\Phi_2/\partial x\|_{x=0} = 0$ and $-\kappa_{\text{eff,p}} \partial\Phi_2/\partial x\|_{x=l_{p^-}} = -\kappa_{\text{eff,s}} \partial\Phi_2/\partial x\|_{x=l_{p^-}}$
	3	$\sigma_{\text{eff,p}} \partial^2\Phi_1/\partial x^2 = a_p F j_p$	$\partial\Phi_1/\partial x\|_{x=0} = -I/\sigma_{\text{eff,p}}$ and $-\sigma_{\text{eff,p}} \partial\Phi_1/\partial x\|_{x=l_p} = 0$
	4	$\partial c_s/\partial t = D_{s,p}/r^2 \, \partial/\partial r(r^2 \partial c_s/\partial r)$ Initial condition $c_s\|_{t=0} = 0.5 c_{s,\max,p}$	$\partial c_s/\partial r\|_{r=0} = 0$ and $j_p = -D_{s,p} \partial c_s/\partial r\|_{r=R_p}$
Separator	5	$\varepsilon_s \partial c/\partial t = D_{\text{eff,s}} \partial^2 c/\partial x^2$	$-D_{\text{eff,p}} \partial c/\partial x\|_{x=l_{p^-}} = -D_{\text{eff,s}} \partial c/\partial x\|_{x=l_{p^+}}$ and $-D_{\text{eff,s}} \partial c/\partial x\|_{x=l_{p^+l_{s^-}}} = -D_{\text{eff,n}} \partial c/\partial x\|_{x=l_{p^+l_{s^+}}}$
	6	$I = -\kappa_{\text{eff,s}} \partial\Phi_2/\partial x + 2\kappa_{\text{eff,s}} RT/F(1-t_+) \partial \ln c/\partial x$	$-\kappa_{\text{eff,p}} \partial\Phi_2/\partial x\|_{x=l_{p^-}} = -\kappa_{\text{eff,s}} \partial\Phi_2/\partial x\|_{x=l_{p^+}}$ and $-\kappa_{\text{eff,s}} \partial\Phi_2/\partial x\|_{x=l_{p^+l_{s^-}}} = -\kappa_{\text{eff,n}} \partial\Phi_2/\partial x\|_{x=l_{p^+l_{s^+}}}$
Negative electrode	7	$\varepsilon_n \partial c/\partial t = D_{\text{eff,n}} \partial^2 c/\partial x^2 + a_n(1-t_+) j_n$ Initial condition $c\|_{t=0} = c_0$	$-D_{\text{eff,s}} \partial c/\partial x\|_{x=l_p+l_{s^-}} = -D_{\text{eff,n}} \partial c/\partial x\|_{x=l_p+l_{s^+}}$ and $-D_{\text{eff,n}} \partial c/\partial x\|_{x=l_p+l_s+l_n} = 0$
	8	$-\sigma_{\text{eff,n}} \partial\Phi_1/\partial x - \kappa_{\text{eff,n}} \partial\Phi_2/\partial x + 2\kappa_{\text{eff,n}} RT/F(1-t_+) \partial \ln c/\partial x = I$	$-\kappa_{\text{eff,s}} \partial\Phi_2/\partial x\|_{x=l_p+l_{s^-}} = -\kappa_{\text{eff,n}} \partial\Phi_2/\partial x\|_{x=l_p+l_{s^+}}$ and $\Phi_2\|_{x=l_p+l_s+l_n} = 0$
	9	$\sigma_{\text{eff,n}} \partial^2\Phi_1/\partial x^2 = a_n F j_n$	$-\sigma_{\text{eff,n}} \partial\Phi_1/\partial x\|_{x=l_p+l_s} = 0$ and $\partial\Phi_1/\partial x\|_{x=l_p+l_s+l_n} = -I/\sigma_{\text{eff,n}}$
	10	$\partial c_s/\partial t = D_{s,n}/r^2 \, \partial/\partial r(r^2 \partial c_s/\partial r)$ Initial condition $c_s\|_{t=0} = 0.85 c_{s,\max,n}$	$\partial c_s/\partial r\|_{r=0} = 0$ and $j_n = -D_{s,n} \partial c_s/\partial r\|_{r=R_n}$

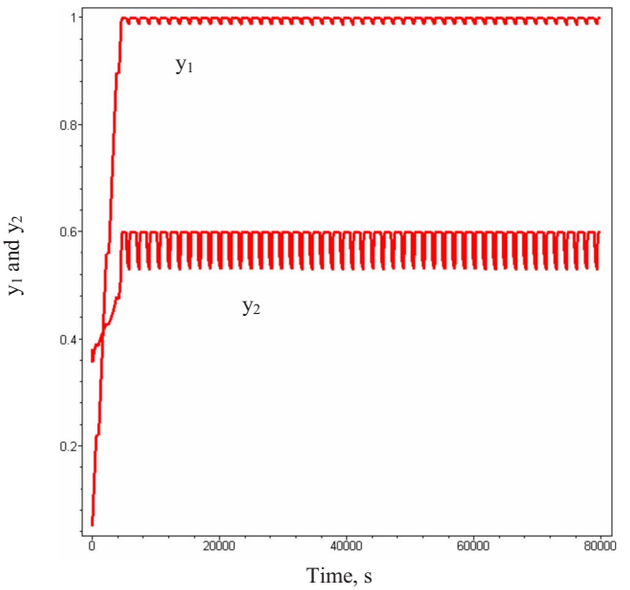

Figure 4. (Color online) Concentration and potential distributions from the cycling of galvanostatic charge/open-circuit/discharge processes of a thin-film electrode.

distribution through the depth of the electrode is considered and solved concomitantly with the solid-phase diffusion.

A comparison between the simulation of a single discharge curve using the BAND(J) [1-4] approach and a similar approach using the polynomial profile approximation for the solid-phase concentration shows that the computation time needed is less for the former. They are 2.5 s for the former and 6 s for the latter. Figure 6 compares the results from the simulation of one cycle (consists of charge and discharge processes) using both the continuum representation and the BAND(J) approaches. It can be observed from this plot that the cycling behavior predictions agree for both approaches. But the computation time taken by the proposed approach is only 15 s, whereas BAND(J) requires 45 s.[28] Though the BAND(J) approach is a linear equation solver that may be implemented for either the discrete time or the continuum representations of the boundary condition, comparisons are made between the BAND(J) approach and the proposed continuum representation to indicate the need for powerful nonlinear DAE solvers. Moreover, the BAND(J) approach is considered as the state-of-the-art approach in the numerical simula-

Table III. Expressions used in the lithium-ion battery model given by Table II.

$\kappa_{\text{eff,i}} = \varepsilon_i^{\text{Brugg}_i}(4.1253 \times 10^{-2} + 5.007 \times 10^{-4} c - 4.7212 \times 10^{-7} c^2 + 1.5094 \times 10^{-10} c^3 - 1.6018 \times 10^{-14} c^4)$ i = p,s,n

$\sigma_{\text{eff,i}} = \sigma_i(1 - \varepsilon_i - \varepsilon_{\text{f,i}})$ i = p,n

$D_{\text{eff,i}} = D\varepsilon_i^{\text{Brugg}_i}$ i = p,s,n

$a_i = 3/R_i(1 - \varepsilon_i - \varepsilon_{\text{f,i}})$ i = p,n

$j_p = 2k_p(c_{s,\max,p} - c_{s,p}\|_{r=R_p})^{0.5} c_{s,p}\|_{r=R_p}^{0.5} c^{0.5} \sinh[0.5F/RT(\Phi_1 - \Phi_2 - U_p)]$

$U_p = -4.656 + 88.669\theta_p^2 - 401.119\theta_p^4 + 342.909\theta_p^6 - 462.471\theta_p^8 + 433.434\theta_p^{10}/-1.0 + 18.933\theta_p^2 - 79.532\theta_p^4 + 37.311\theta_p^6 - 73.083\theta_p^8 + 95.96\theta_p^{10}$,
where $\theta_p = c_{s,p}\|_{r=R_p}/c_{s,p,\max}$

$j_n = 2k_n(c_{s,\max,n} - c_{s,n}\|_{r=R_n})^{0.5} c_{s,n}\|_{r=R_n}^{0.5} c^{0.5} \sinh[0.5F/RT(\Phi_1 - \Phi_2 - U_n + FR_{\text{SEI}} j_n)]$

$U_n = 0.7222 + 0.1387\theta_n + 0.029\theta_n^{0.5} - 0.0172/\theta_n + 0.0019/\theta_n^{1.5} + 0.2808 \exp(0.90 - 15\theta_n) - 0.7984 \exp(0.4465\theta_n - 0.4108)$, where $\theta_n = c_{s,n}\|_{r=R_n}/c_{s,n,\max}$

Table IV. Parameters used for the simulation ($LiCoO_2$ and LiC_6 system).

Symbol	Unit	Positive electrode	Separator	Negative electrode
σ_i	S/m	100		100
$\varepsilon_{f,i}$		0.025		0.0326
ε_i		0.385	0.724	0.485
Brugg			4	
$D_{s,i}$	m^2/s	1.0×10^{-14}		3.9×10^{-14}
D	m^2/s		7.5×10^{-10}	
k_i	$mol/(s\ m^2)/(mol/m^3)^{1+\alpha a,i}$	2.334×10^{-11}		5.0307×10^{-11}
$c_{s,i,max}$	mol/m^3	51554		30,555
$c_{s,i0}$	mol/m^3	$0.4955 \times 51,554$		$0.8551 \times 30,555$
C_0	mol/m^3		1000	
R_p	m	2.0×10^{-6}		2.0×10^{-6}
l_i	m	80×10^{-6}	25×10^{-6}	88×10^{-6}
R_{SEI}	$\Omega \cdot m^2$			0.0
T_+			0.363	
F	C/mol		96487	
R	J/(mol K)		8.314	
T	K		298.15	

tion of a battery that is available as open source. To summarize, the continuum representation of discrete processes is three times more efficient than the current approach for cycling studies with respect to the computation speed.

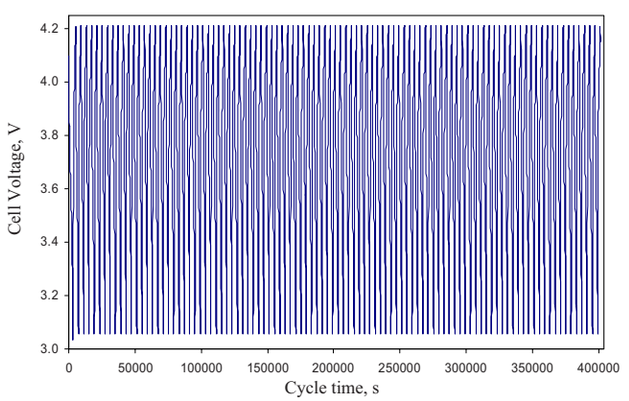

Figure 5. (Color online) Charge/discharge cycles of a pseudo-two-dimensional lithium-ion battery model for 100 cycles.

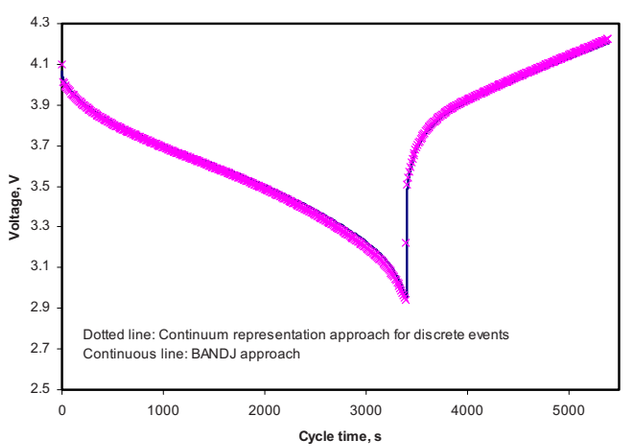

Figure 6. (Color online) Comparison of the continuum representation approach with the current BAND(J) approach for cycle 1 of the pseudo-two-dimensional lithium-ion battery model.

State Detection

It can be observed from the battery modeling literature that the prior mentioning of process time for cycling parameters such as charge, discharge, or open circuit is not an option during battery operations. This is because of the physical and chemical properties that change inside the battery that result in battery degradation or capacity fade. To have this continuum representation technique valid for this situation, it requires a similar mathematical representation as a function of the state variables such as the solid-phase surface concentration of the active electrode materials against the independent variable time. This would be a useful tool to predict the cycle life of batteries.

The continuum representation as a function of the state variable to detect state variation was attempted and was successful in the solid-phase diffusion model. Figure 7 shows the current, potential, and concentration distributions at various times for five cycles of charge, open-circuit, and discharge for the solid-phase diffusion model. However, advanced mathematical techniques are further needed to implement the same for other two illustrative models discussed. The limitations are mainly because of (*i*) complexity in the mathematical derivation of a constraint using state-detecting variables that can automate the cycling studies and (*ii*) DAE solver failures while introducing a stiff constraint for state variables such as the solid-phase surface concentration. This can be addressed by carefully deriving an alternate constraint with less stiffness or nonlinearity. This also needs the evaluation of the consistent initial conditions for all the algebraic components of the resulting DAE system to avoid solver failures.

Conclusion

In this study, a continuum representation of the discrete events in the charge/discharge cycle of a battery has been proposed. It has been established that initialization is not required between the discrete events of a given cycle or between any two cycles. The proposed method is based on the generally followed protocol for a particular battery chemistry and can be altered for other widely used protocols to utilize it in different battery systems. This technique works well for most of the possible battery models if the duration for each discrete event in a cycle is fixed, though it is not the practical case. However, the method has advantages, such as the complete automation of cycling data to predict the cycle behavior and the lesser computational cost when compared to existing conventional methods.

This approach is more useful if the above limitation is overcome by expressing the additional equations as functions of the state variables, such as the state-of-charge, which is a key state detecting

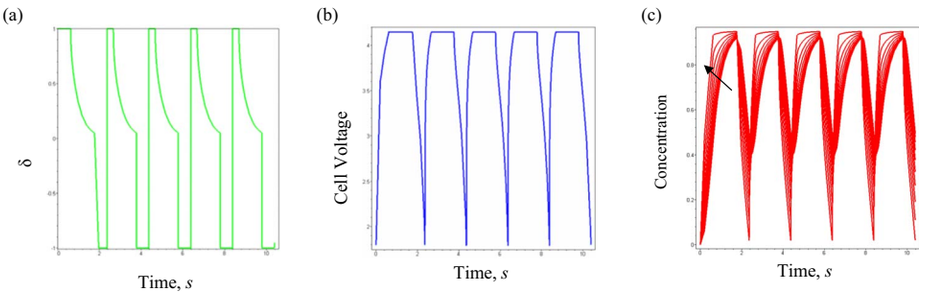

Figure 7. (Color online) (a) Current distribution, (b) potential distribution, and (c) concentration distribution for a solid-phase diffusion model simulated as a function of the state variable. The arrow mark in (c) represents the increasing time steps. The cycling protocol is similar to that in Fig. 2 and thus has three segments in each plot indicating the constant current charge, the constant potential charge, and the constant current discharge.

variable. This shifts from one process to the other at a specified cutoff potential without additional information on the predefined duration for each cycling parameter. Future work will involve the implementation of a mathematical expression for a full-order model as a function of state variables and thus will enable the cycling of battery models in milliseconds or lesser time.

Acknowledgments

We are thankful for the partial financial support of this work by the Oronzio de Nora Industrial Electrochemistry Postdoctoral Fellowship of The Electrochemical Society, the National Science Foundation (CBET-0828002), and the U.S. government.

Washington University assisted in meeting the publication costs of this article.

List of Symbols

a_i	specific surface area of electrode i (i = p, n), m^2/m^3
$Brugg_i$	Bruggeman coefficient of region i (i = p, s, n)
c	electrolyte concentration, mol/m^3
c_0	initial electrolyte concentration, mol/m^3
$c_{s,i}$	concentration of lithium ions in the intercalation particle of electrode i (i = p, n), mol/m^3
$c_{s,i,0}$	initial concentration of lithium ions in the intercalation particle of electrode i (i = p, n), mol/m^3
$c_{s,i,max}$	maximum concentration of lithium ions in the intercalation particle of electrode i (i = p, n), mol/m^3
D	electrolyte diffusion coefficient, m^2/s
$D_{s,i}$	lithium ion diffusion coefficient in the intercalation particle of electrode i (i = p, n), m^2/s
F	Faraday's constant, C/mol
i_1	solid-phase current density, A/m^2
i_2	solution phase current density, A/m^2
I	applied current density, A/cm^2
j_i	wall flux of Li^+ on the intercalation particle of electrode i (i = n, p), mol/m^2 s
k_i	intercalation/deintercalation reaction rate constant of electrode i (i = p, n), $mol/(mol/m^3)^{1.5}$
l_i	thickness of region i (i = p, s, n), m
n	negative electrode
p	positive electrode
r	radial coordinate, m
R	universal gas constant, J/(mol K)
R_i	radius of the intercalation particle of electrode i (i = p, n), m
R_{SEI}	initial solid electrolyte interface layer resistance at the negative electrode, Ω m^2
s	separator
t_+	Li^+ transference number in the electrolyte
T	absolute temperature, K
U_i	open-circuit potential of electrode i (i = p, n), V
x	spatial coordinate, m

Greek

ε_i	porosity of region i (i = p, s, n)
$\varepsilon_{f,i}$	volume fraction of the fillers of electrode i (i = p, n)
θ_i	dimensionless concentration of lithium ions in the intercalation particle of electrode i ($\theta_i = c_{s,i}/c_{s,i,max}$)
κ	ionic conductivity of the electrolyte, S/m
$\kappa_{eff,i}$	effective ionic conductivity of the electrolyte in region i (i = p, s, n), S/m
σ_i	electronic conductivity of the solid phase of electrode i (i = p, n), S/m
$\sigma_{eff,i}$	effective electronic conductivity of the solid phase of electrode i (i = p, n), S/m
Φ_1	solid-phase potential, V
Φ_2	electrolyte phase potential, V

References

1. T. F. Fuller, M. Doyle, and J. Newman, *J. Electrochem. Soc.*, **141**, 1 (1994).
2. J. Newman, M. Doyle, and J. Reimers, *J. Power Sources*, **52**, 211 (1995).
3. M. Doyle and J. Newman, *J. Power Sources*, **54**, 46 (1995).
4. M. Doyle and J. Newman, *J. Appl. Electrochem.*, **27**, 846 (1997).
5. P. Arora, R. E. White, and M. Doyle, *J. Electrochem. Soc.*, **145**, 3647 (1998).
6. G. G. Botte, V. R. Subramanian, and R. E. White, *Electrochim. Acta*, **45**, 2595 (2000).
7. P. Ramadass, B. Haran, R. E. White, and B. N. Popov, *J. Power Sources*, **111**, 210 (2002).
8. R. Spotnitz, *J. Power Sources*, **113**, 72 (2003).
9. P. Ramadass, B. Haran, P. M. Gomadam, R. E. White, and B. N. Popov, *J. Electrochem. Soc.*, **151**, A196 (2004).
10. S. Santhanagopalan, Q. Guo, P. Ramadass, and R. E. White, *J. Power Sources*, **156**, 620 (2006).
11. V. Boovaragavan and V. R. Subramanian, *Electrochem. Commun.*, **9**, 1772 (2007).
12. B. Wu and R. E. White, *Comput. Chem. Eng.*, **25**, 301 (2001).
13. T. Van Nguyen, Ph.D. Thesis, Texas A&M University, College Station, TX (1988).
14. V. R. Subramanian, V. D. Diwakar, and D. Tapriyal, *J. Electrochem. Soc.*, **152**, A2002 (2005).
15. V. R. Subramanian, V. Boovaragavan, and V. D. Diwakar, *Electrochem. Solid-State Lett.*, **10**, A255 (2007).
16. V. R. Subramanian, V. Boovaragavan, V. Ramadesigan, and M. Arabandi, *J. Electrochem. Soc.*, **156**, A260 (2009).
17. K. E. Brenan, S. L. Campbell, and L. R. Petzold, *Numerical Solution of Initial-Value Problems in Differential-Algebraic Equations*, North-Holland, New York (1989).
18. P. N. Brown, A. C. Hindmarsh, and L. R. Petzold, *A Description of DASPK: A Solver for Large-Scale Differential-Algebraic Systems*, Lawrence Livermore National Laboratory, UCRL, Livermore, CA (1992).
19. D. Manca, G. Buzzi-Ferraris, T. Faravelli, and E. Ranzi, *Combust. Theory Modell.*, **5**, 185 (2001).
20. P. Deuflhard and U. Nowak, SFB 123, Technical Report no. 332, University of Heidelberg, Heidelberg, Germany (1985).
21. http://www.numericatech.com/jacobian.htm, last accessed April 8, 2009.
22. http://www.psenterprise.com/gproms/, last accessed April 8, 2009.
23. I. Bauer, F. Finocchi, W. J. Duschl, H.-P. Gail, and J. P. Schlöder, *Astron. Astrophys.*, **317**, 273 (1997).
24. M. Berzins and R. M. Furzeland, Report no. TNER.85.058, Shell Research Limited, Thornton Research Centre, Chester, U.K. (1985).
25. T. J. R. Hughes, *Comput. Methods Appl. Mech. Eng.*, **127**, 387 (1995).
26. J. Geiser, *J. Eng. Math.*, **57**, 79 (2007).
27. T. Osaka, S. Nakade, M. Rajamaki, and T. Momma, *J. Power Sources*, **119-121**, 929 (2003).
28. http://www.cchem.berkeley.edu/jsngrp/, last accessed April 8, 2009.